⌘ *Author's Choice*

Ablation of Vacuole Protein Sorting 18 (*Vps18*) Gene Leads to Neurodegeneration and Impaired Neuronal Migration by Disrupting Multiple Vesicle Transport Pathways to Lysosomes*⑤◆

Chao Peng[‡§], **Jian Ye**[‡§], **Shunfei Yan**[‡§], **Shanshan Kong**[‡§], **Ye Shen**[‡], **Chenyu Li**[‡], **Qinyu Li**[¶], **Yufang Zheng**[¶], **Kejing Deng**[‡], **Tian Xu**[‡‖1], **and Wufan Tao**[‡§2]

From the ‡Institute of Developmental Biology and Molecular Medicine, §State Key Laboratory of Genetic Engineering, and ¶Department of Physiology and Biophysics, School of Life Science, Fudan University, Shanghai 200433, China and the ‖Howard Hughes Medical Institute, Department of Genetics, Yale University School of Medicine, New Haven, Connecticut 06536

Background: The physiological function of *Vps18* in mammals is unknown.

Results: Deleting *Vps18* in mice leads to neurodegeneration by disrupting multiple vesicle transport pathways to lysosomes and impairs neuron migration via accumulation of β1 integrin.

Conclusion: *Vps18* contributes to neuron survival and migration.

Significance: This study demonstrates the critical functions of *Vps18*-mediated vesicle transport pathways in mammalian brain development.

Intracellular vesicle transport pathways are critical for neuronal survival and central nervous system development. The Vps-C complex regulates multiple vesicle transport pathways to the lysosome in lower organisms. However, little is known regarding its physiological function in mammals. We deleted *Vps18*, a central member of Vps-C core complex, in neural cells by generating *Vps18^{F/F}*; Nestin-*Cre* mice (*Vps18* conditional knock-out mice). These mice displayed severe neurodegeneration and neuronal migration defects. Mechanistic studies revealed that *Vps18* deficiency caused neurodegeneration by blocking multiple vesicle transport pathways to the lysosome, including autophagy, endocytosis, and biosynthetic pathways. Our study also showed that ablation of *Vps18* resulted in up-regulation of β1 integrin in mouse brain probably due to lysosome dysfunction but had no effects on the reelin pathway, expression of N-cadherin, or activation of JNK, which are implicated in the regulation of neuronal migration. Finally, we demonstrated that knocking down β1 integrin partially rescued the migration defects, suggesting that *Vps18* deficiency-mediated up-regulation of β1 integrin may contribute to the defect of neuronal migration in the *Vps18*-deficient brain. Our results demonstrate important roles of *Vps18* in neuron survival and migration, which are disrupted in multiple neural disorders.

Lysosome-related biological processes play important roles in neurodegenerative diseases. The endocytosis and autophagy are two major lysosome-related vesicle transport pathways (1, 2). Endocytic dysfunction has been documented in a surprising range of neurodegenerative diseases such as Alzheimer disease (3). Ablation of autophagy causes neurodegeneration in mice, demonstrating the importance of autophagy in neuron survival (4, 5). Furthermore, the mutation of lysosomal hydrolases such as cathepsin D, B, or L, which impairs substrate degradation, also leads to neurodegeneration in mammals (6, 7).

During vertebrate brain development, coordinated migration of neurons from the ventricular zone to the cortical plate is essential for the formation of proper brain structure (8). Reelin regulates the migration of neurons along the radial glial fiber network through binding to its receptors, VLDLR/ApoER2, and activating DAB1 adapter (9, 10). Cell surface adhesion molecules, such as the α3β1 integrin, can also modulate neuronal migration, although α3 or β1 integrin deficiency does not affect cortical layer formation (11–13). Recently, endocytic pathways were found to regulate neuronal migration. Knocking down *Rab5* or *Rab11* in mouse cerebral cortex disturbs neuronal migration via up-regulating N-cadherin and decreasing JNK activity (14).

Membrane tethering mediated by large tethering factors is the first step for vesicle fusion. The Vps18 protein is a central subunit of Vps-C core complex, which is also composed of Vps11, Vps16, and Vps33. Vps-C complexes function as tethering factors in late endosome- and lysosome-related vesicle fusion processes in lower eukaryotic organisms. Vps-C complex deficiency in yeast results in the loss of vacuole structure

and accumulation of autophagosomes and late endosomes (15, 16). Mutation of *dor*, a *Drosophila* homologue of *Vps18*, causes a complete lack of pigmentation and the existence of exaggerated multivesicular structure in retinal cells, blockage of autophagosome-lysosome fusion in larval fat body, and promotion of tumor metastasis (17–19). *Vps18* mutation in zebrafish results in hepatomegaly and skin hypopigmentation (20, 21). In cultured mammalian cells, disturbance of *Vps18* function blocks autophagosome-lysosome as well as early endosome fusion (22, 23). However, the physiological role(s) of *Vps18* are still unknown in mammals.

Here we generated the *Vps18*-deficient mice and studied the mutant phenotypes and the underlying mechanisms. Although conventional homozygous *Vps18* mutants were embryonic or early postnatal lethal, neural-specific *Vps18*-deficient mice displayed serious growth retardation and died before P12.[3] Our study showed that loss of *Vps18* led to widespread neurodegeneration resulting from blocking multiple vesicle transport pathways to the lysosome, including autophagy, endocytosis, and biosynthetic pathways. Surprisingly, we also found that *Vps18* deficiency impairs neuronal migration. Further analyses revealed that migration defect may result from accumulation of $\beta 1$ integrin on the cell surface. Our study demonstrates the critical functions of *Vps18* in neuron survival and migration in mammals.

EXPERIMENTAL PROCEDURES

Generation of Vps18-deficient Mice—The genomic clones containing exons 2–5 of the *Vps18* gene were isolated from a 129sv mouse genomic phage library (Stratagene). The *Vps18* gene was modified by adding loxP sequences to EcoRV and ScaI sites flanking exons 3–4. A β-gal reporter gene with a splicing acceptor and a neomycin expression cassette flanked by FLP recombination target (FRT) sites was inserted into the EcoRV site. The neomycin and diphtheria toxin expression cassettes were used as positive and negative selection markers, respectively. Gene targeting was carried out in the W4 ES cell line (ES-W4129S6, Taconic Transgenic). Chimeric mice were bred with C57BL to generate $Vps18^{+/galeo}$ mice. $Vps18^{+/galeo}$ mice were bred with the PGK-*Flp* transgenic mice (stock number 003946, The Jackson Laboratory) with 129/Sv genetic background to remove the β-gal reporter and PGK-*Neo* expression cassettes to establish $Vps18^{+/F}$ mice. Progenies were genotyped by PCR using a set of *Vps18*-specific oligonucleotides: Vps18-F2: 5′-ATCAAACTCAGACATCAGGTGCG-3′ and *Vps18*-R2 5′-CAAGTCAATGCTGTAAGGGCAAG-3′.

To mutate the *Vps18* gene in neural cells, $Vps18^{+/F}$; Nestin-*Cre* mice were generated by breeding $Vps18^{+/F}$ mice with Nestin-*Cre* transgenic mice (Stock Number 003771, The Jackson Laboratory) with C57BL/6J genetic background. Finally, $Vps18^{F/F}$; Nestin-*Cre* (*Vps18* conditional knock-out (CKO)) mice were produced by crossing $Vps18^{+/F}$; Nestin-*Cre* with $Vps18^{F/F}$ mice. All mice mentioned above were maintained on C57BL and 129/Sv mixed genetic background. To specifically

mutate the *Vps18* gene in Purkinje cells, $Vps18^{+/F}$ mice were backcrossed C57BL six times and then crossed with Pcp2-*Cre* transgenic mice (Stock Number 004146, The Jackson Laboratory) with C57BL genetic background to generate $Vps18^{F/F}$; Pcp2-*Cre* mice. Progenies were genotyped by PCR using oligonucleotides specific for *Vps18* (*Vps18*-F2 and *Vps18*-R2) and *Cre* (Cre-F1: 5′-GGAAAATGCTTCTGTCCGTTTG-3′ and Cre-R2: 5′-CGCATAACCAGTGAAACAGCATTGC-3′), respectively. All experiments were performed in accordance with protocols approved by the Animal Care and Use Committee of the Institute of Developmental Biology and Molecular Medicine at Fudan University.

Southern Blot—Genomic DNA was extracted from targeted ES clones and digested with restriction enzyme XbaI. Southern blot analysis was performed as described previously (24). A 1025-bp DNA fragment containing part of exon2 of the *Vps18* gene was amplified by PCR, labeled by ^{32}P, and used as probe. PCR primers are: *Vps18*-southern F1, GATCTAAGCCCCAGGCCTTT, and *Vps18*-southern R1, ACGAGGCTAGTGATCCGCTC.

RT-PCR—Total mRNAs were isolated from P4 mouse brain using TRIzol (Invitrogen). cDNAs were reverse-transcribed using an TaKaRa RT-PCR (avian myeloblastosis virus) kit, version 3.0, and amplified with the combination of specific primers for *Vps18* exon 4 or for GAPDH gene as internal control. They are: for exon 4 of *Vps18*, 5′-TGGATGATGGGAGATGGAGTGC-3′ and 5′-CCAGCAGCAGTAGGAAATGGAAC-3′, and for GAPDH gene, 5′-TGTTCCTACCCCCAATGTGTCC-3′ and 5′-GGAGTTGCTGAAGAAGTCGCAG-3′.

PCR Assay for Vps18 Deletion in Genomic DNA—Genomic DNA was isolated from P4 mouse brain. Real-time PCR was performed with $2\times$ HotSybr PCR reaction mix (NuStar Laboratory) on an Mx3000P quantitative PCR system (Stratagene) following the manufacturer's instructions. GAPDH was used as the base-line standard for real-time PCR. The primers for *Vps18* are the same as those used in RT-PCR. The primers for GAPDH gene are 5′-GGAAGTCCAGGGCTACATTCTATCC-3′ and 5′-CAGTGCTGTCCAACAAGTGAGTCTC-3′.

Western Blot—Proteins from whole mouse brains or specific brain regions were extracted by radioimmune precipitation assay buffer with freshly added 1 mM PMSF and $1\times$ proteinase inhibitor (Roche Applied Science). The proteins were resolved on SDS-PAGE followed by Western blotting with antibodies against the following proteins: caspase-3 (9662), LC3 (2775), and cleaved Notch 1 (Val-1744) from Cell Signaling Technology; cathepsin D (sc-6486) and Rab7 (sc-10767) from Santa Cruz Biotechnology; Dab1 (AB5840, Chemicon), Eea1 (610456), and Rab11 (610657) from BD Transduction Laboratories; and Rab4 (ab13252; Abcam) and ubiquitin (Z 0458; DakoCytomation). The same amounts of proteins were used for the control probed for GAPDH (KC-5G4; KangChen).

Histological, Immunohistochemical, and Immunofluorescent (IF) Analyses—For frozen sections, mouse brains were dissected out, fixed in 4% paraformaldehyde, and dehydrated in 30% sucrose overnight at 4 °C consecutively and then embedded in OCT and frozen in liquid nitrogen-cooled isopentane. Sections were then collected at 12 and 60 μm respectively. 12-μm sections were used for histological, immunohistochem-

---

[3] The abbreviations used are: P, postnatal day; E, embryonic day; CKO, conditional knock-out; Ctrl, control; IF, immunofluorescent; EYFP, enhanced yellow fluorescent protein; GFAP, glial fibrillary acidic protein; LC3, light chain 3.
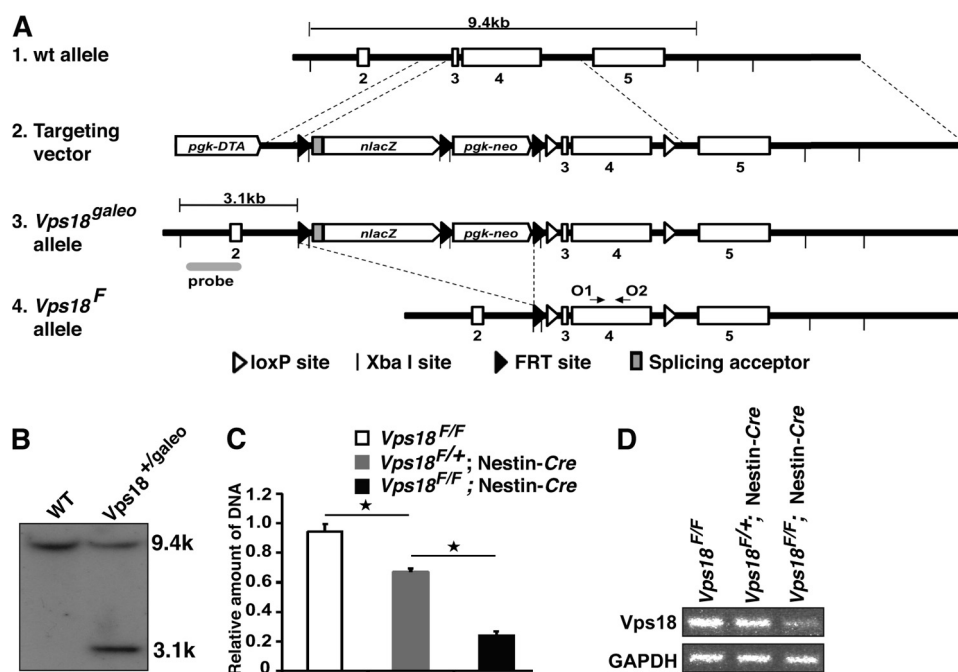
FIGURE 1. **Generation of *Vps18* conditional knock-out mice.** *A*, schematic representation of the knock-out strategy for *Vps18* gene. *Panel 1*, genomic DNA fragment of *Vps18* gene containing exons 2–5. *Panel 2*, schematic structure of the *Vps18* targeting vector. *Panel 3*, genomic structure of *Vps18*^{galeo} allele after homologous recombination. *Panel 4*, genomic structure of *Vps18*^{F} allele after removal of *nLacZ* and PGK-neomycin expression cassettes simultaneously by FLP. *pgk-DTA* and *pgk-Neo* represent the diphtheria toxin A and the neomycin expression cassettes, respectively. *nLacZ* represents a modified *Escherichia coli* β-galactosidase gene containing nuclear localization signal at its N-terminal. The exons are numbered and depicted by *open boxes*. The *open* and *black triangles* denote loxP and FLP recombination target (FRT) sequence, respectively. The *gray box* before *nLacZ* represents a splicing acceptor. XbaI sites are indicated by *short vertical lines*. The *gray ellipse* in *panel 3* depicts the probe for Southern blot analysis. *B*, Southern blot analysis of genomic DNA extracted from targeted ES clones. The 9.4- and 3.1-kb XbaI fragments represent WT and modified alleles respectively. *C* and *D*, efficiency of *Vps18* deletion in the *Vps18* CKO mouse brain. Deletion efficiency of *Vps18* gene was estimated at the DNA level by real-time PCR (*C*) and transcriptional level by RT-PCR analyses (*D*). The genomic DNA and total RNA prepared from P4 *Vps18* CKO or Ctrl mouse brains were used for templates. O1 and O2 (*arrows* in *A*) specific to exon 4 of *Vps18* were primers for PCR. Assay shown is representative of three experiments with similar results. Values in *C* represent the means ± S.E. of three separate experiments. *, *p* value < 0.001.

ical, and IF analyses. 60-µm sections were used for IF staining to analyze radial glial fibers.

For histological analysis, the sections were stained with hematoxylin and eosin. For immunohistochemistry and IF analysis, the sections were stained with antibodies against the following proteins: calbindin (C9848; Sigma); GFAP (MAB3402), LC3 (ab58610), and Tbr1 (ab31940) (all from Abcam); LAMP1 (553792; Pharmingen); Nestin (MAB353; Chemicon); and Cux1 (sc-13024; Santa Cruz Biotechnology) using the standard protocols (25). Fluorescence micrographs were acquired using a Leica DMRXA2 fluorescence microscope equipped with a Leica DFC350FX camera or Zeiss LSM710 confocal microscope. Histochemical micrographs were acquired using a Leica DMRXA2 fluorescence microscope equipped with a Leica DFC300FX camera. Images were processed using Adobe Photoshop.

Electron Microscopy—Samples were sliced into $2 \times 2 \times 2$ mm, fixed in a fixative consisting of 2% glutaraldehyde and 4% paraformaldehyde, and rinsed in the phosphate buffer. Following a postfixation for 2 h with 1% osmium tetroxide in phosphate buffer at 4 °C, they were dehydrated and embedded in resin. Ultrathin sections were prepared using a Reichert ultramicrotome, contrasted with uranyl acetate and lead citrate, and examined under a Philips CM120 electron microscope.

Flow Cytometry—Fluorescence-activated cell sorter (FACS) analysis for expression of β1 integrin was carried out as previously described (12). Briefly, cerebral cortex, hippocampus, and cerebellum were dissected from E16.5 brains, minced, and treated in trypsin. Then, cells were dissociated mechanically and incubated with biotin-conjugated anti-β1 integrin antibody (13-0291; eBioscience) and then with FITC conjugated-streptavidin, and analyzed with the BD FACSCalibur Flow Cytometer (BD Biosciences). Both *Vps18* CKO and Ctrl neural cells incubated with FITC conjugated-streptavidin only were used for blank control.

In Utero Electroporation—*In utero* electroporation was carried out following standard protocols (26). Plasmids expressing shRNA and mCherry or EYFP alone were injected into the lateral ventricles of mouse embryos at E14. Five days after electroporation, embryos were collected for analysis. The shRNA targets for β1 integrin and scramble shRNA (sh-scr) were described previously (27) and were cloned into a pRUEM vector under the control of U6 promoter. The shRNA targets for β1 integrin were GGAAGGAAATCTTAGCTTT.

Statistical Analysis—Unpaired Student's *t* test was used. A value of *, *p* < 0.05, **, *p* < 0.01 or ***, *p* < 0.001 denoted statistical significance.

RESULTS

The Vps18 Gene Is Essential for Mouse Development—We first generated *Vps18* mutant allele, *Vps18*^{galeo} (Fig. 1*A*, *panel 3*), in mouse embryonic stem cells using a "conventional first and conditional ready" gene-targeting strategy (28). In the targeting vector, a β-*gal* reporter gene with a splicing acceptor and
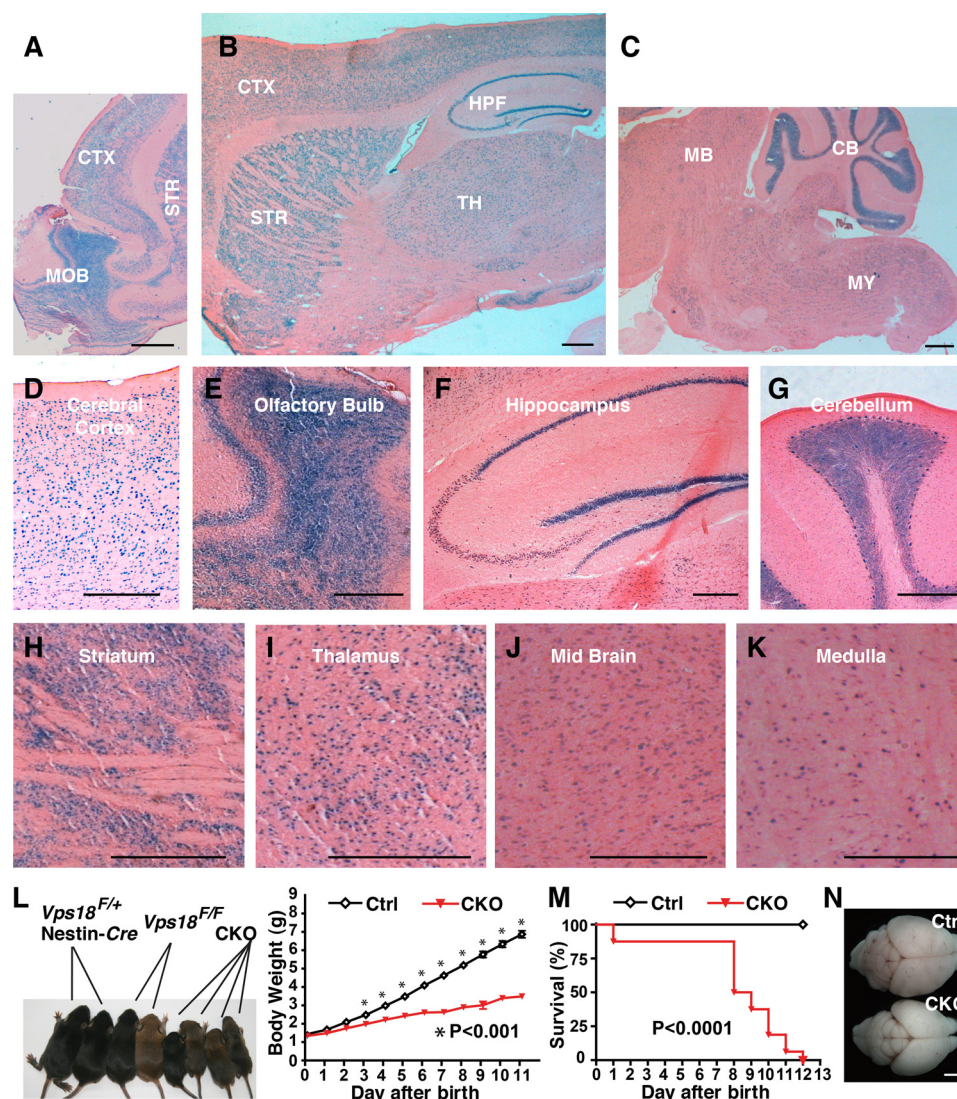
FIGURE 2. **Vps18 expression pattern in the $Vps18^{+/galeo}$ mouse brains and postnatal lethality and growth retardation of the $Vps18$ CKO mice.** *A–C*, X-gal staining of sagittal sections of the $Vps18^{+/galeo}$ mouse brain reveals wide expression of $Vps18$ in various mouse brain regions, especially with intensive signals in olfactory bulb (*MOB*), cerebral cortex (*CTX*), striatum (*STR*), hippocampus (*HPF*), thalamus (*TH*), and cerebellum (*CB*). *MB*, mid brain; *MY*, brain stem. *D–K*, higher magnification micrographs of different parts of $Vps18^{+/galeo}$ brain in *A–C*. *L*, representative photograph of the CKO and Ctrl pups at P10 from the same litter (*left panel*) and body weight development of the mutant and control mice (*right panel*). *M*, Kaplan-Meier survival curve of the $Vps18$ CKO and Ctrl mice ($n \geq 16$ for all genotypes). *N*, the mutants display smaller cerebrums and cerebellums than their littermates. Image is representative of mouse brains from six mice per group. Ctrl in *L* and *M* include $Vps18^{F/F}$ and $Vps18^{+/F}$ mice. Values in *L* represent the means $\pm$ S.E. of body weight ($n \geq 16$ for all genotypes). (*Scale bar*: 400 μm (*A–C*); 200 μm (*D–K*); 2 mm (*N*).)

a neomycin expression cassette flanked by FLP recombination target (FRT) sites were inserted after exon 2. Exons 3 and 4 were flanked by loxP sites (Fig. 1*A*, and see "Experimental Procedures"). Homologous recombinants containing the mutant allele were identified by PCR and verified by Southern blot (Fig. 1*B*) using the probe shown in Fig. 1*A*, *panel 3*. The targeted ES clones were injected into C57BL/6 blastocysts to generate $Vps18^{+/galeo}$ mice. In these mice, the expression of β-gal reporter is under the control of the endogenous $Vps18$ gene promoter, and β-gal reporter is in-frame fused with the first 78 amino acids of Vps18 protein after splicing. Therefore, the expression pattern of $Vps18$ can be examined in $Vps18^{+/galeo}$ mice using β-gal as a reporter. Our analyses showed that $Vps18$ was highly expressed in various brain regions including cerebral cortex, cerebellum, thalamus, striatum, etc. (Fig. 2, *A–K*). When $Vps18^{+/galeo}$ mice were intercrossed, no viable

$Vps18^{galeo/galeo}$ offspring were detected at postnatal day 7 (P7). Cumulative genotyping of P7 live mice indicated that $Vps18^{+/+}$ and $Vps18^{+/galeo}$ mice were recovered at a ratio close to 1:2 (71:151), suggesting that $Vps18$ deficiency results in embryonic or early postnatal lethality.

Growth Retardation and Postnatal Death of $Vps18^{F/F}$; Nestin-Cre Mice—Because $Vps18$ is highly expressed in mouse brain tissues (Fig. 2, *A–K*), we decided to investigate the physiological function of $Vps18$ in the central nervous system first. We generated floxed $Vps18$ allele (thereafter called $Vps18^{F}$, Fig. 1*A*, *panel 4*) by crossing the $Vps18^{+/galeo}$ mice with PGK-*Flp* transgenic mice to remove the β-gal reporter gene and the neomycin expression cassette from the $Vps18^{galeo}$ allele. $Vps18^{F/F}$ mice were further crossed with Nestin-*Cre* transgenic mice to produce $Vps18^{F/F}$; Nestin-*Cre* mice (referred to as $Vps18$ CKO), in which exons 3 and 4 of the $Vps18$ gene were specifically

deleted in neural cells. This deletion resulted in a frameshift and an early stop codon in exon 5. Real-time PCR analysis showed that ~80% of *Vps18* gene was deleted in the *Vps18* CKO brain cells (Fig. 1*C*). This was also further confirmed at the transcriptional level by RT-PCR (Fig. 1*D*).

Both the *Vps18*[F/+]; Nestin-*Cre* and the *Vps18*[F/F] mice grow normally (Fig. 2*L*). Thereafter, *Vps18*[F/F] mice (referred to as Ctrl) were used for control unless specified. The *Vps18* CKO mice were viable at birth and indistinguishable in appearance from their *Vps18*[F/+]; Nestin-*Cre* or *Vps18*[F/F] littermates. However, all *Vps18* CKO mice died before P12 (Fig. 2*M*). Further analyses showed that the *Vps18* CKO mice displayed severe postnatal growth retardation and were apparently smaller at P10 (Fig. 2*L*). Consistent with their reduced body weight, the brains of the *Vps18* CKO mice were also smaller, especially in the cerebral cortex and cerebellum region, than their littermates at P10 (Figs. 2*N* and 3*D*).

Severe Neurodegeneration due to Neural-specific Vps18 Deficiency—To further investigate the function of *Vps18* in the development of mouse brain, we prepared histological sections from P1 and P10 mouse brains. Characteristic differences between the *Vps18* CKO and Ctrl are shown in Fig. 3, *A* and *B*, in the hippocampus and in Fig. 3, *C* and *D*, in the cerebellum. At P1 the morphological structures of hippocampus from the mutant mice were similar to that of the Ctrl, except that CA3 region was split into two layers, and neurons were more loosely associated (Fig. 3*A*, *right panel*, indicated by *arrow* and *arrowhead*, respectively). However, at P10, the mutant hippocampus completely lost its morphological structure (Fig. 3*B*, *right panel*), suggesting a dramatic loss of neurons, a character of neurodegeneration, in the *Vps18* CKO mice at P10.

Discernible differences between the mutant and Ctrl mice were also present in cerebellums. Histological analyses showed that the cerebellum of the *Vps18* CKO mice at P1 was a little smaller and less foliated than that of littermate controls (Fig. 3*C*), indicating a prenatal developmental retardation in the *Vps18* CKO mice. The cerebellum of the *Vps18* CKO mice at P10 was not only less foliated but also much smaller when compared with that of the Ctrl (Fig. 3*D*). The smaller size of the *Vps18* CKO cerebellum could be a result of neurodegeneration, but it also could be due to the defect of cell proliferation. To ascertain whether *Vps18* deficiency would lead to loss of neural cells in cerebellum, we generated *Vps18*[F/F]; Pcp2-*Cre* mice, in which *Vps18* would be deleted specifically in Purkinje cells after P6 (29). Purkinje cells are generated between E11 and E13 and complete their radial migration between E13 and E18 (30). Therefore, deletion of *Vps18* should have no effects on proliferation of Purkinje cells *in Vps18*[F/F]; Pcp2-*Cre* mice. We observed a dramatic loss of Purkinje cells at the age of 1 month (Fig. 3*E*, *left two panels*) and only few Purkinje cells at the age of 3 months in *Vps18*[F/F]; Pcp2-*Cre* mice (Fig. 3*E*, *right two panels*), demonstrating the critical function of *Vps18* in Purkinje cell survival. This result also suggests that *Vps18*-deficient neurons die in a cell-autonomous fashion.

To further confirm the presence of neuronal damage in the *Vps18* CKO mice and to examine whether loss of neural cells was caused by apoptosis, we evaluated the expression of GFAP and activation of caspase-3 in the *Vps18* CKO brain. IF staining with anti-GFAP antibody showed increased GFAP signaling in almost all regions of P10 *Vps18* CKO brain, *e.g.* cerebral cortex, hippocampus, and cerebellum (Fig. 3, *G–I*), suggesting widespread neuronal damage. We also found that the number of caspase-3-positive cells markedly increased in many regions of the mutant brain such as the cerebral cortex, hippocampus, and cerebellum (Fig. 3, *J–L*). The protein level of activated caspase-3 in the *Vps18* CKO brain at P4 was also dramatically elevated when compared with that of the Ctrl (Fig. 3*F*), indicating that *Vps18*-deficient neurons die through apoptosis. Altogether, these results demonstrate that the lack of *Vps18* in neural cells leads to serious neurodegeneration in mice.

Blockage of the Autophagy and Endocytosis Pathways in the Vps18 CKO Mice—The autophagy pathway, endocytosis pathway, and lysosome function are critical for neuron survival (4, 5, 7, 31, 32). To investigate the mechanisms underlying neurodegeneration phenotype in the *Vps18* CKO mice, we evaluated the effects of *Vps18* deficiency on autophagy and endocytosis pathways and lysosome function.

First, we studied the effect of *Vps18* deficiency on autophagy pathway. LC3 exists in two forms (cytosolic LC3-I and membrane-bound LC3-II), and LC3-II is a marker for autophagosomes (33). Our analysis showed that there was an increase in the protein levels of both LC3-II and LC3-I (Fig. 4*A*). In addition, many cells displayed a higher intensity of LC3 signals in the *Vps18* CKO mouse brain (Fig. 4*E*). Furthermore, electronic microscopy revealed that autophagosomes were dramatically accumulated in the *Vps18*-deficient neurons (Fig. 5, *B*, *D*, and *E*). These results suggest that *Vps18* deficiency may lead to a blockage of autophagosome clearance or an enhancement of autophagosome formation. To distinguish these two possibilities, we examined whether there was an accumulation of ubiquitinated proteins in the *Vps18* CKO brain by immunohistochemistry and Western blot with anti-ubiquitin antibody. Loss of autophagy but not enhancement of autophagosome formation leads to accumulation of diffuse ubiquitinated proteins in the cytosol followed by the generation of inclusion bodies (5, 34). Both our immunohistochemistry and our Western blot analyses showed that the amount of ubiquitinated proteins dramatically increased in the *Vps18* CKO mouse brain (Fig. 4, *B* and *F*). Ubiquitin-containing inclusion bodies were also observed in many parts of the *Vps18* CKO brain (Fig. 4*F*, *arrows*). The *p62* gene is required for inclusion body formation (35). Co-IF staining with ubiquitin and p62 antibodies revealed that the ubiquitin-containing inclusion bodies in P10 *Vps18* CKO brain were positive for p62 (Fig. 4*G*, *arrows*). Therefore, we conclude that *Vps18* is critical for autophagosome clearance in the mouse brain.

Next, we investigated the effect of *Vps18* deficiency on the endocytosis pathway. Western blot analysis showed that both Eea1 and Rab7 proteins, markers for early and late endosomes, respectively, were accumulated in *Vps18* CKO mouse brain. However, the protein levels of Rab4 and Rab11, which are involved in fast and slow recycling pathways via recycling endosomes, respectively, were not altered (Fig. 4*C*). Lamp1 is a marker for late endosomes/lysosomes. IF staining with anti-Lamp1 antibody showed much stronger signals of Lamp1 in the
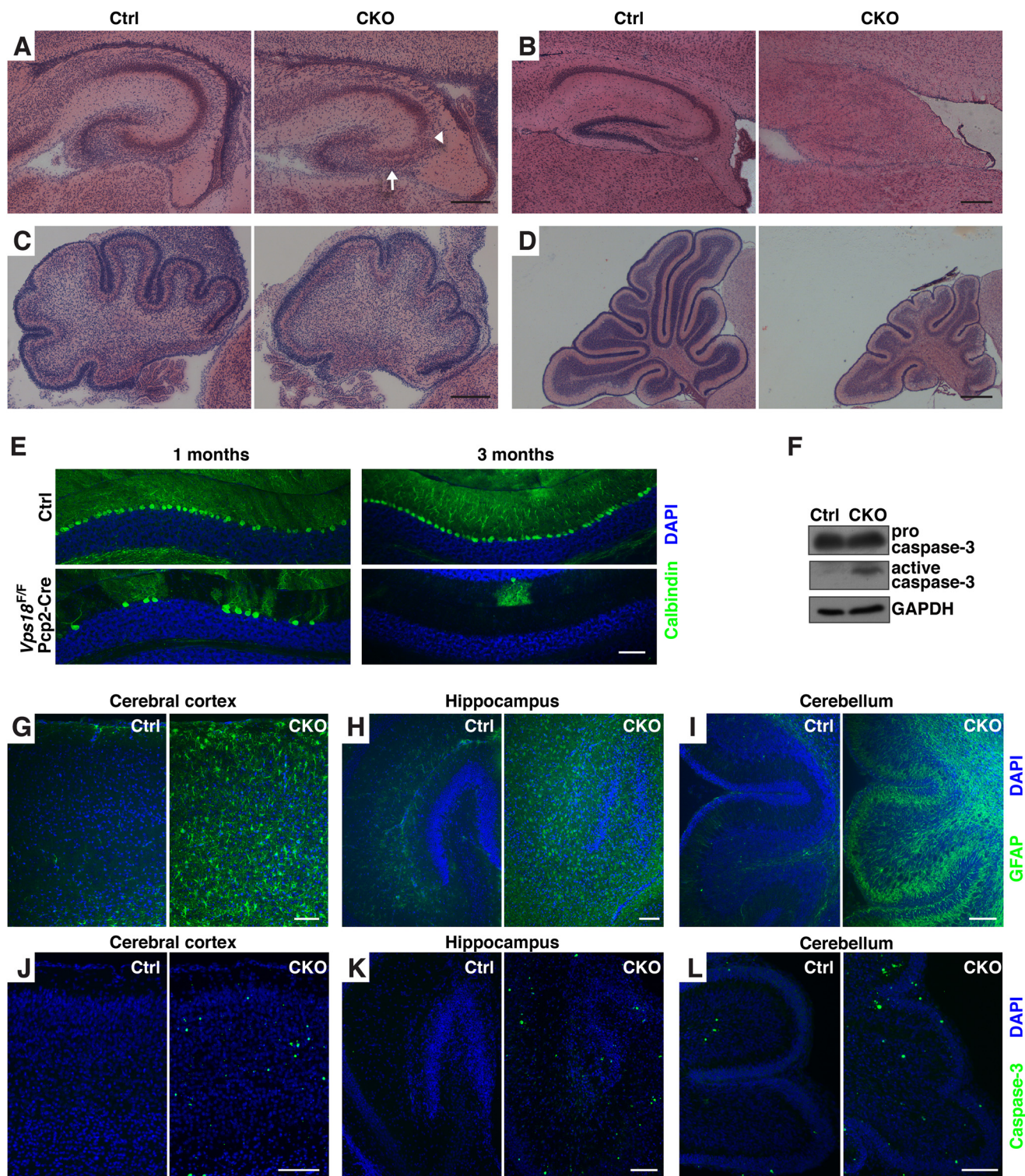
FIGURE 3. **Neurodegeneration in the *Vps18* CKO mouse brains.** *A–D*, histological analyses of the hippocampus and cerebellum of the *Vps18* CKO mice. *A* and *B*, disruption of the morphological structures of hippocampus in the *Vps18* CKO mice at P10 due to significant cell loss. *Arrow* and *arrowhead* in *A* indicate the split and neuron/loosely associated CA3 region separately. *C* and *D*, less foliation and a smaller size of the *Vps18* CKO cerebellum. Sagittal cryosections of the indicated mouse brains at P1 (*A* and *C*) or P10 (*B* and *D*) were stained with H&E and microphotographed. *E*, dramatic loss of the Purkinje cells in the *Vps18*^F/F^; Pcp2-*Cre* mice. The cryosections of the indicated mouse cerebellums were stained with anti-calbindin. *F*, Western blot analysis of total proteins from P4 brains discloses activation of caspase-3. Blot shown is representative of three experiments with similar results. *G–I*, a striking increase of GFAP signals in cerebral cortex (*G*), hippocampus (*H*), and cerebellum (*I*) of P10 *Vps18* CKO mouse brain. *J–L*, Increased apoptotic cells in the *Vps18* CKO brains. Cryosections of the cerebral cortex (*J*), hippocampus (*K*), and cerebellum (*L*) from the indicated mice at P10 were stained with anti-caspase-3. All images are representative brain sections from at least three mice per group. (*Scale bar*: 200 μm (*A–D*); 100 μm (*E* and *G–L*).)
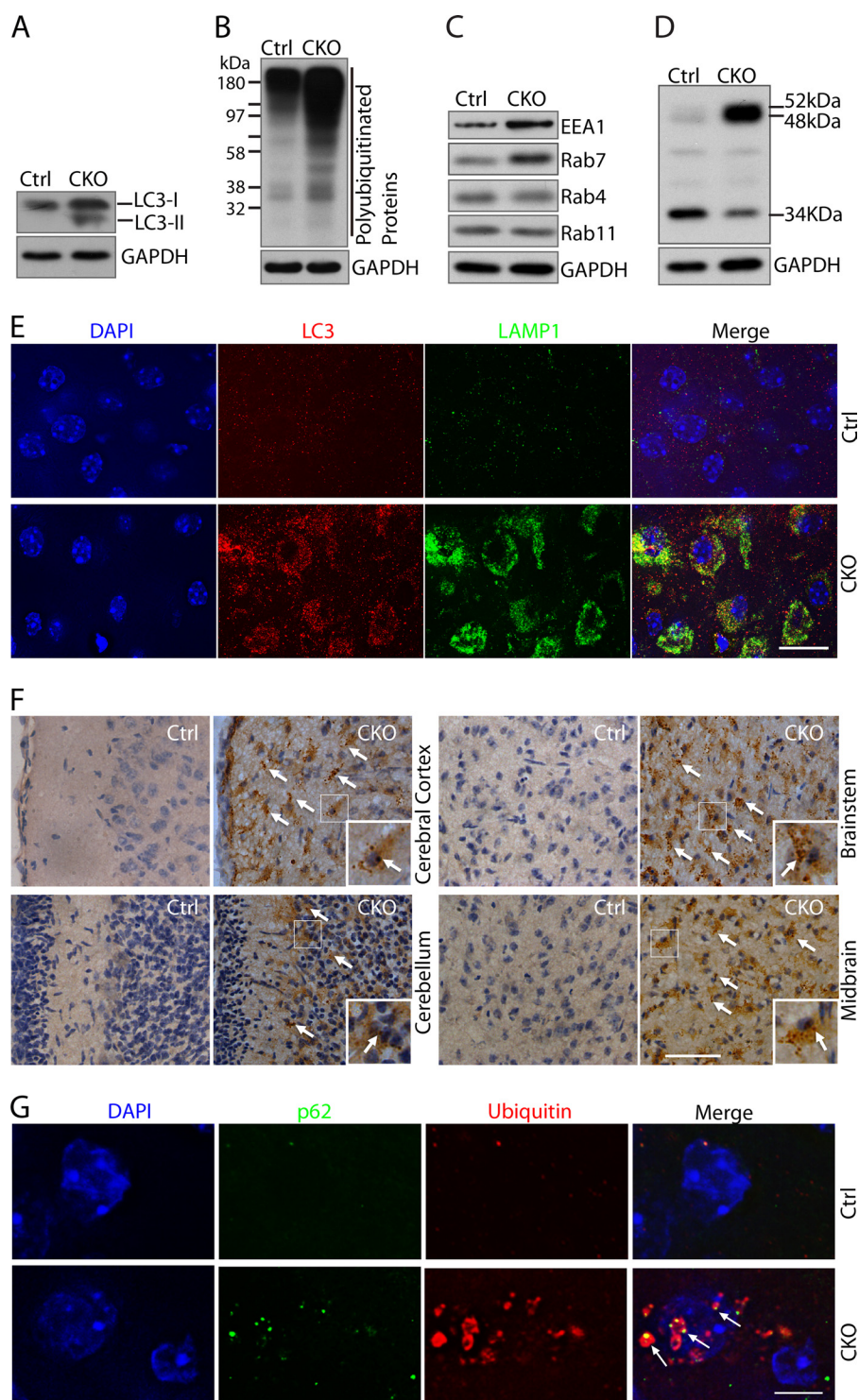
FIGURE 4. **Blockage of autophagosome clearance and maturation of endosome and lysosomal proteases in the *Vps18* CKO brains.** *A–D*, Western blot analyses of proteins or markers involved in autophagy, endocytosis, and biosynthetic pathways using the cell lysates prepared from the whole brain of the *Vps18* CKO and Ctrl mouse at P10. *A* and *B*, the accumulation of both forms of LC3 (LC3-I and LC3-II) (*A*) and ubiquitinated proteins (*B*). *C*, an increased expression of EEA1 and Rab7, but not Rab4 and Rab11. *D*, a dramatic accumulation of immature cathepsin D (52 and 48 kDa) and a marked reduction of the matured form (34 kDa). Total proteins were extracted from the *Vps18* CKO or Ctrl mouse brains and blotted with the indicated antibodies. *E*, the accumulation of autophagosomes and lysosome/late endosomes in the *Vps18* CKO brain cells. Cryosections of cerebral cortex from the indicated mice were immunofluorescently stained with anti-LC3 and anti-LAMP1. *F*, buildup of ubiquitin-positive inclusions in the *Vps18* CKO brains at P10. Cryosections of various indicated brain tissues from *Vps18* CKO and Ctrl mice were immunohistochemically stained with anti-ubiquitin antibody. *Insets* are enlarged views of the cropped regions. *Arrows* indicate ubiquitin-positive inclusions. *G*, co-IF staining with anti-ubiquitin and anti-p62 antibodies shows that ubiquitin-containing inclusion bodies in P10 *Vps18*-deficient brain cells are also positive for p62. *Arrows* indicate colocalized signals of ubiquitin and p62. Blots shown are representatives of three experiments with similar results. Images shown are representative mouse brain sections from at least three mice per group. (*Scale bar*: 20 μm (*E*); 50 μm (*F*); 5 μm (*G*).)
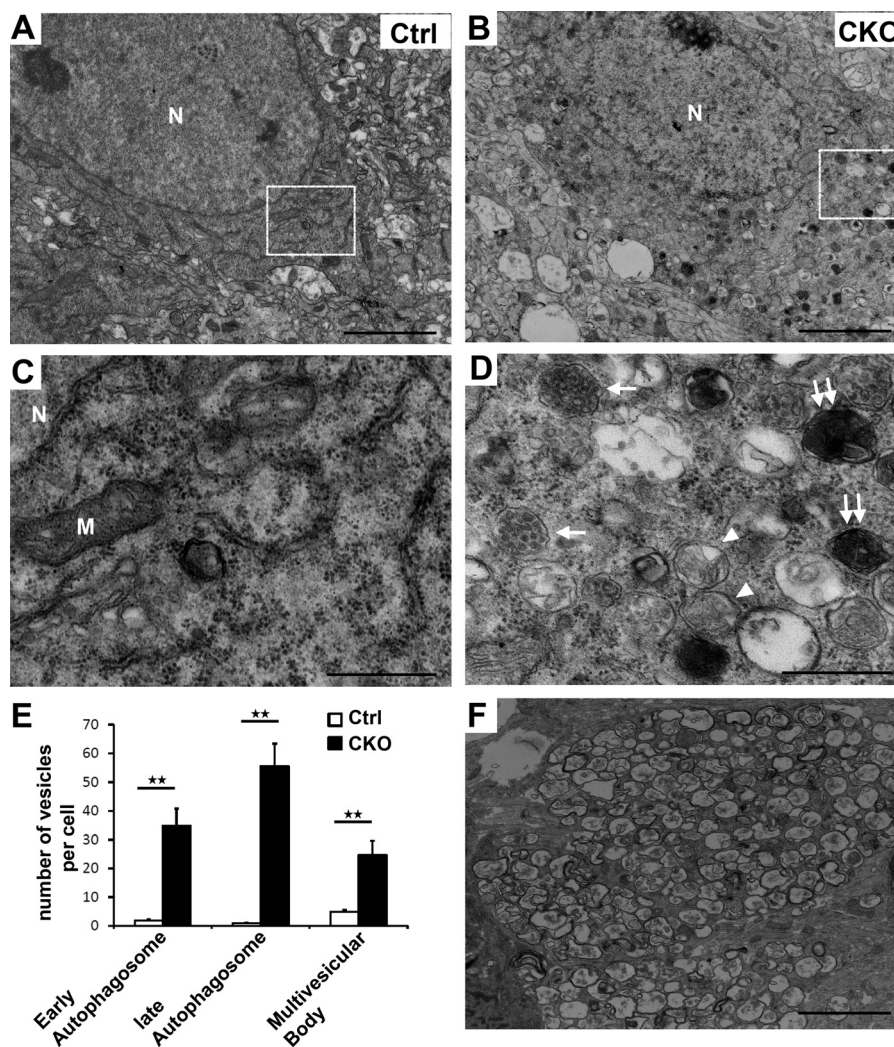
FIGURE 5. **The accumulation of autophagosomes, late endosomes, and amorphous densely stained vesicles in the *Vps18* CKO mouse brain.** *A* and *B*, typical electron micrographs of Ctrl or *Vps18* CKO cortical neuron at P10. *C* and *D*, enlarged view of the cropped region in *A* and *B*. *Arrowheads*, early autophagosomes; *double arrows*, late autophagosomes; *arrows*, multivesicular bodies. *N* and *M* in *A–C* represent nucleus and mitochondria respectively. *E*, bar graph shows great accumulation of early and late autophagosomes and multivesicular bodies in the *Vps18* CKO cerebral cortex. The organelles in 13 randomly chosen neurons on electronic microscope photographs from two sets of mouse brains were counted. *F*, electron microscopy analysis reveals that enormously swollen dystrophic neurites in the *Vps18* CKO hippocampus are full of amorphous, multilaminar body-like vesicles. Images are representative mouse brain sections from at least three mice per group. Values in *E* represent the means ± S.E. **, *p* value < 0.01. (*Scale bar*: 2 μm (*A*, *B*, and *F*); 500 nm (*C* and *D*).)

Vps18 CKO mouse brain (Fig. 4*E*). Furthermore, electronic microscopy revealed that multivesicular bodies (late endosome) were dramatically accumulated in the *Vps18*-deficient neurons (Fig. 5, *B*, *D*, and *E*). All these data demonstrate that early endosome maturation and late endosome degradation are disturbed in the *Vps18* CKO mouse brain.

Finally, we evaluated the maturation of lysosomal proteases in the *Vps18* CKO mice. Cathepsin D is a major type of lysosome protease. It is synthesized as a pre-proenzyme and undergoes several steps of proteolytic processing to become a mature enzyme after being transported to late endosome/lysosome. We found that the pre-proform (52 kDa) and intermediate form (48 kDa) of cathepsin D accumulated in the *Vps18* CKO mouse brain, whereas the mature form (34 kDa) decreased (Fig. 4*D*). This result indicates that the maturation of lysosomal proteases is impaired in the *Vps18* CKO mouse brain, which will lead to lysosome dysfunction. In conclusion, the results presented illustrate that the autophagy pathway, endocytosis path-

way, and lysosomal enzyme maturation are disturbed in the *Vps18* CKO mouse brain, strongly suggesting that serious neurodegeneration phenotype in the *Vps18* CKO mice is likely a result of the disturbance of these vesicle transport pathways.

Impaired Neural Cell Migration in the Vps18 CKO Mice—Impaired neural cell migration is another intriguing mutant phenotype that we have observed in the *Vps18* CKO mouse brain. This mutant phenotype was first revealed by our observation that the CA3 region of the hippocampus in the *Vps18* CKO mouse brain was split into two layers (indicated in Fig. 3*A*, *right panel*, by the *arrow*). Next we examined whether *Vps18* deficiency affected neuronal migration in cerebral cortex. IF staining with anti-Cux-1 (a layer II–IV marker) and Tbr1 (a layer VI and subplate marker) did not show obvious laminar abnormalities in P1 *Vps18* CKO cerebral cortex (data not shown). However, IF staining with antibodies described above may not be sensitive enough to detect some minor defects of neuronal migration. To ascertain whether *Vps18* deficiency
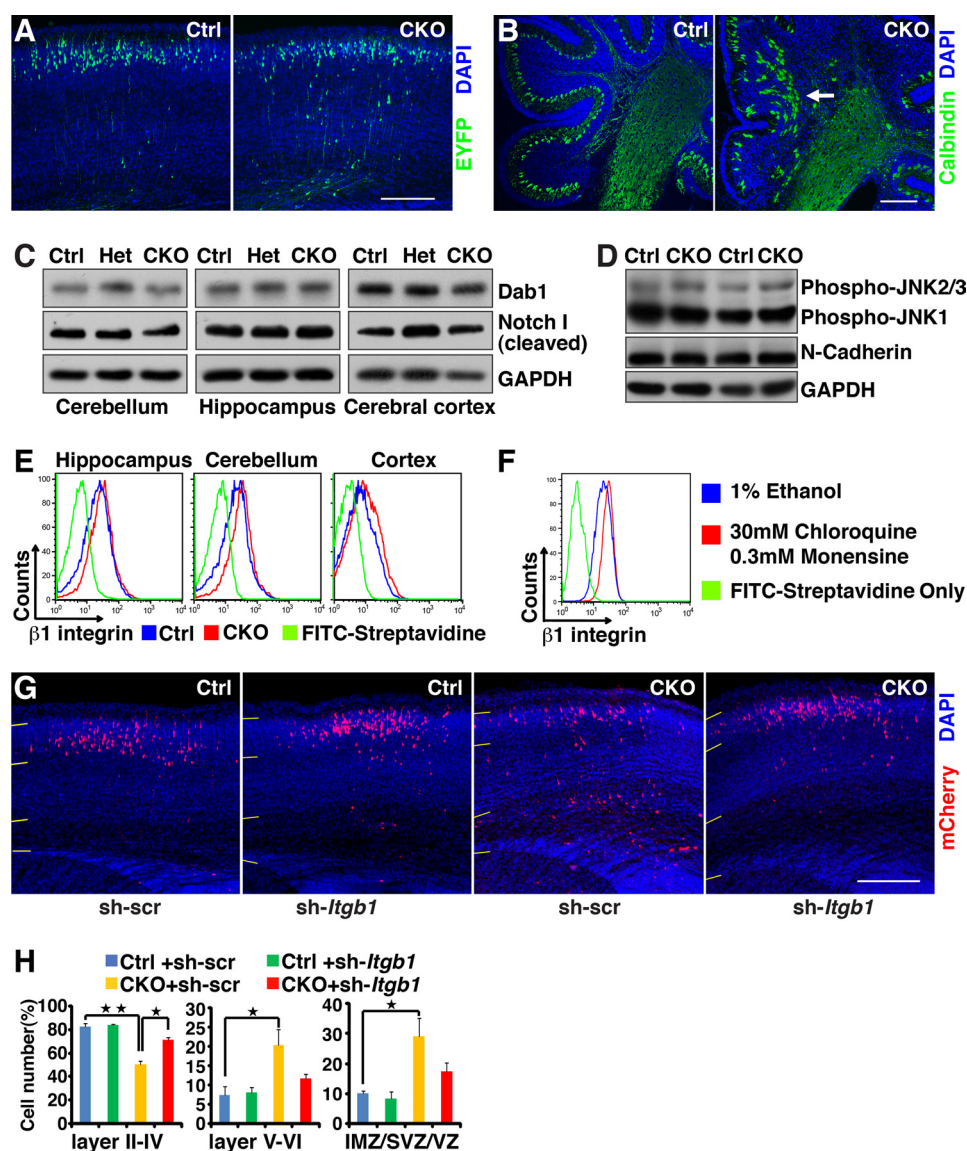
FIGURE 6. **Vps18 deficiency-mediated impairment of neuronal migration and up-regulation of β1 integrin on cell surfaces.** *A*, representative images of E19 cerebral cortices of the indicated mice electroporated at E14 with plasmid p*EYFP*. A fraction of EYFP-positive cortical neurons was abnormally located in the intermediate zone and subventrical zone in the *Vps18* CKO cerebral cortex. *B*, sagittal cryosections of cerebellums from the indicated mice were stained with anti-calbindin. An *arrow* indicates abnormal localized Purkinje cells under inner granule cell layer in the *Vps18* CKO cerebellum. *C* and *D*, Western blot analysis reveals no change in the protein levels of Dab1, cleaved Notch I, N-cadherin, and activated JNKs in the indicated regions of E17 CKO mouse brains when compared with the controls. *Het*: *Vps18*[+/F]; Nestin-*Cre*. Blots shown are representatives of three experiments with similar results. *E*, The FACS profiles showing an increase of β1 integrin expression on the surface of the E16.5 *Vps18* CKO brain cells as indicated. *F*, the FACS profiles demonstrating the accumulation of β1 integrin on the surface of NIH3T3 cells treated with the lysosomal inhibitors, chloroquine and monensin. *G* and *H*, knockdown of β1 integrin partially rescued the migration defect in the *Vps18* CKO brain. Representative images in *G* are from the section of E19 *Vps18* CKO or Ctrl cerebral cortices electroporated with the plasmids co-expressing *mCherry* and indicated shRNA. The graphs in *H* show the estimation of cell migration in distinct regions of the cerebral cortices in the images as shown in *G*. Values represent the means ± S.E. of percentage of cell number. Seven images (sections)/brain and three brains for each set of experiments were used for counting mCherry-positive cells. All images are representative mouse brain sections from at least three mice per group. The FACS profiles shown are representative of three experiments with similar results. *IMZ/SVZ/VZ*: intermediate zone/subventricular zone/ventricular zone. *Short yellow bars* in *G* indicate the borders between layers II–IV and V–VI of the cortical plate, and intermediate zone/subventricular zone/ventricular zone. sh-scr, scrambled shRNA; sh-*Itgb1*, β1 integrin shRNA. *, *p* value < 0.05, **, *p* value < 0.01. (*Scale bar*: 200 μm.)

affects neural cell migration in cerebral cortices, we performed *in utero* electroporation with the plasmid p*EYFP* at E14 and visualized the EYFP-labeled cells at E19. The results showed that although almost all control EYFP^{+} cells migrated normally to layers II–IV of the cortical plate, a fraction of *Vps18*-deficient EYFP^{+} cells tailed in layers V–VI, the intermediate zone, or the subventrical zone. This was a clear indicator of defective neuronal migration in the cerebral cortex (Fig. 6*A*). Furthermore, we observed a more severe migration defect in the *Vps18*-defi-

cient cerebellum. IF staining with anti-calbindin showed that *Vps18* deficiency resulted in disruption of Purkinje cell layer formation. Purkinje cells in P10 control cerebellum had assembled into a single tight layer above inner granule cell layer; in contrast, Purkinje cells in some areas of *Vps18*-deficient cerebellum were still located under the inner granule cell layer (Fig. 6*B*, *arrow*) in addition to their lower density distribution. All these results demonstrate that *Vps18* deficiency impairs neural cell migration in cerebral cortex, hippocampus, and cerebellum.

Vps18 Deficiency Does Not Disturb the Reelin Pathway, Expression of N-cadherin, or Activation of JNK—During cortical development, the reelin pathway plays critical roles in regulating radial migration of neurons (9, 10). The cell surface protein levels of two reelin receptors, VLDLR and ApoER2, are regulated by endocytosis (36). Thus, *Vps18* deficiency may affect reelin signaling by disturbing the endocytosis process of VLDLR and ApoER2 in neural cells. To test this possibility, we evaluated the expression of Dab1, a direct target of reelin receptors, in *Vps18* CKO mice. The accumulation of Dab1 is a hallmark of defects in reelin signaling. However, there was no accumulation of Dab1 in the hippocampus, cerebral cortex, or cerebellum of the mutant mice examined by Western blot (Fig. 6*C*). To ascertain that the activity of Dab1 was not altered, we also examined the level of the cleaved form of Notch intracellular domain (Notch ICD), which is directly regulated by Dab1 (37), and found that it was also not altered in the *Vps18* CKO brain (Fig. 6*C*). These results indicate that the reelin pathway may not be affected in *Vps18* CKO brains.

Recently, *Rab5/11*-mediated early endocytic pathway has been demonstrated to play an important role in neuronal migration through regulating N-cadherin expression and JNK activity (14). Therefore, we evaluated the protein level of N-cadherin and JNK activity in the *Vps18* CKO brain. Western blot analysis showed that the protein level of N-cadherin or phosphorylation of JNK in *Vps18* CKO brains was similar to that of Ctrl (Fig. 6*D*), suggesting that *Vps18* deficiency did not affect N-cadherin expression or JNK activity. In summary, the above results suggest that neuronal migration defects in *Vps18* CKO mice may not be caused by disturbing the reelin pathway or early endocytosis.

The Up-regulation of β1 Integrin Disturbed Neuronal Migration in Vps18 CKO Mice—Integrins are another major family of adhesion molecules. β1 integrin is expressed in primary neurons and has been implicated in regulation of neuronal migration (12, 13, 38, 39). Integrins were suggested to be trafficked to lysosomes for degradation (40). Based on these previous studies, we hypothesized that *Vps18* deficiency-mediated blockage of endosome-lysosome pathway may impair neuron migration by up-regulating β1 integrin. To test our hypothesis, we first investigated whether the expression of β1 integrin was affected in the *Vps18* CKO brain. We found that the cell surface level of β1 integrin was increased in *Vps18* mutant cells when compared with that of controls by FACS (Fig. 6*E*), demonstrating that *Vps18* deficiency results in up-regulation of β1 integrin in the *Vps18* CKO brain. Next, we further asked whether the accumulation of β1 integrin on the cell surface was caused by blockage of lysosome function. NIH3T3 cells were treated with chloroquine and monensin, two lysosome inhibitors, to block lysosome pathway followed by FACS analysis. Indeed, the results showed that treated cells displayed a higher level of β1 integrin on the cell surface (Fig. 6*F*), demonstrating that lysosome dysfunction would lead to an increase of β1 integrin on the cell surface.

To further verify whether up-regulating expression of β1 integrin on the cell surface is responsible for the defects of neuronal migration in the *Vps18* CKO mouse brain, we knocked down β1 integrin in the *Vps18*-deficient neural cells by shRNA

using *in utero* electroporation. The results showed that reducing expression of β1 integrin partially rescued migration defects of the *Vps18*-deficient neural cells (Fig. 6, *G* and *H*), illustrating that *Vps18* deficiency-mediated up-regulation of β1 integrin in *Vps18*-deficient neural cells is one of the reasons for their impaired migration behavior (see "Discussion").

DISCUSSION

Although the function of the *Vps18* gene has been extensively studied in lower organisms, its physiological function in mammals remains unknown. Here we have illustrated the *in vivo* roles of the *Vps18* gene in mammals by ablating the gene in mice. We have shown that *Vps18* deficiency results in embryonic or early postnatal lethality and that neurnal-specific deletion of *Vps18* leads to postnatal lethality and growth retardation. We have for the first time demonstrated that *Vps18* is essential for neuron survival and that loss of *Vps18* led to widespread neurodegeneration in mouse brains. We show here that disruption of *Vps18* in mouse neural cells results in a blockage of endosomal maturation, obstruction of autophagosome clearance, and defective biosynthetic lysosomal trafficking. These studies demonstrate that *Vps18* occupies an essential position in the autophagy, endocytosis, and lysosomal functions in mammals. These studies also illustrate the mechanisms underlying the severe neurodegeneration in *Vps18* CKO mice because it has been well documented that disruption of endocytotic or autophagy pathways or dysfunction of lysosomes lead to neurodegeneration (4, 5, 7, 31, 32). More interestingly, we have also demonstrated that *Vps18* CKO mice displayed defects of neuronal migration in various brain regions including cerebral cortex, hippocampus, and cerebellum. Mechanistic studies revealed that *Vps18* deficiency did not disturb the reelin pathway, JNK activity, or N-cadherin expression, but led to up-regulation of β1 integrin on the cell surface. Furthermore, knockdown of β1 integrin partially rescued the migration defects, thus providing one possible explanation for impaired neuronal migration in the *Vps18* CKO mice.

Although we are currently not able to show the *Vps18* deletion efficiency at the protein level in the *Vps18* CKO brain cells, we have demonstrated that in *Vps18* CKO brain cells, ~80% of *Vps18* gene was deleted at the DNA level by real-time PCR (Fig. 1*C*) and further confirmed that *Vps18* mRNA was significantly reduced by RT-PCR (Fig. 1*D*). These results provide solid evidence that *Vps18* has been efficiently deleted in *Vps18* CKO brain cells. Furthermore, given the very severe phenotypes of the *Vps18* CKO mice, we think that lack of analysis of the *Vps18* deletion efficiency at the protein level in the *Vps18* CKO brain cells will not affect our main conclusion or the significance of our study.

There is evidence indicating that ectopically located neurons can be removed by programmed cell death (41). However, the neurodegeneration phenotype is far more severe than migration defects in *Vps18* CKO mice. For example, most neurons in the hippocampus of *Vps18* CKO mice can migrate correctly, but most of the neurons were lost at P10. In *Vps18^{F/F}*; Pcp2-*Cre* mice, the Purkinje cells can migrate correctly, but most of the Purkinje cells disappeared at the age of 3 months. Therefore, it

seems less likely that neuron migration defect is a major cause of neurodegeneration in *Vps18* CKO mice.

The *p62* gene has been proved to be required for inclusion body formation and is accumulated in autophagy-deficient mice (35). In *Vps18* CKO brains, ubiquitinated proteins were dramatically accumulated and formed inclusion bodies (Fig. 4, *B* and *F*), which were also positive for p62 (Fig. 4*G*). However, Western blot analysis showed that p62 protein level did not increase (data not shown). One possible explanation is that *Vps18*-deficient mice die too early to accumulate sufficient amount of p62 to show an obvious difference through Western blot. These results also indicate that inclusion body formation can happen before the accumulation of p62.

Vps33a also encodes a subunit of Vps-C complex. The buff mutant mouse containing a *Vps33a* point mutation displays reduced Purkinje cell number and smaller size of cerebellum only in old age (>8 and >13–14 months, respectively) (42). However, *Vps18* deficiency results in much more severe defects of mouse brain such as almost complete loss of hippocampus, reduced Purkinje cell number, and impaired neural cell migration at very young age (<P10). There are at least two following possible explanations for these differences. 1) The buff allele of *Vps33a* gene contains a missense mutation and may not completely lose its function. 2) *Vps18* may be more important for the function of the Vps-C complex because loss of *Vps18*, not *Vps33*, leads to the complete disruption of the Vps-C complex in yeast (43).

In the enlarged axons of neurons in Alzheimer disease patients, autophagosomes are highly accumulated. This is believed to result from reduced autophagosome clearance (44, 45). We have observed similar phenotypes in the *Vps18*-deficient mouse brain (Fig. 5*F*). Because the accumulation of autophagosomes in Alzheimer disease patients is thought to contribute to the generation of β-amyloid, we examined whether Aβ 42 is accumulated in *Vps18*-deficient mouse brain. However, we found no difference in the Aβ 42 protein level between the *Vps18* CKO and Ctrl mice (data not shown). This could be due to disturbed maturation of lysosome proteinase such as cathepsin D in *Vps18*-deficient mice because lysosome proteinase was recently suggested to play a role in β-amyloid generation (46). However, we cannot exclude the possibility that *Vps18*-deficient mice die too early to accumulate sufficient β-amyloid because Alzheimer disease is an age-related disease.

It has been recently shown that endocytic pathways play important roles in regulating neuronal migration (14). Suppression of *Rab5*-mediated endocytosis and early endosome formation almost completely blocks neuronal migration in cerebral cortex. Knocking down Rab11 resulted in a phenocopy of Rab5 knockdown. However, deletion of *Vps18* only partially blocks neuronal migration in cerebral cortex and cerebellum and does not change the protein level of Rab4 and Rab11 (Fig. 4*C*), which act downstream of Rab5 and are involved in fast and slow recycling pathways, respectively. Knocking down *Rab5* or *Rab11* resulted in accumulation of N-cadherin and reduction of JNK activity and had no effect on β1 integrin. However, disruption of *Vps18* led to increased expression of β1 integrin on the cell surface but had no effects on N-cadherin and JNK. Thus, *Rab5/Rab11* and *Vps18* regulate neuronal migration by different mechanisms.

Vps18 and *Rab7* are both involved in the regulation of endosome-lysosome fusion, but their effects on neural cell migration are different. Knocking down *Rab7* only blocks the final phase of neuronal migration (14), whereas *Vps18* deficiency impairs the earlier stage of neuronal migration. This discrepancy could be due to the different methods applied. The *Vps18*-deficient cells we studied carry *Vps18*-null mutants, whereas knocking down *Rab7* can only partially block *Rab7* expression. Thus, to the best of our knowledge, *Vps18* deficiency-mediated impairment of neuronal migration provides the first linkage between late endosome/lysosomal function and neuronal migration.

The function of β1 integrin in cell migration during cortical development has been controversial. Cortical neurons are assembled into layers in *Itgb1-CNSko* mice and *Itga3*-null mice (12). However, blocking the function of α3β1 integrins with α3 antibodies perturbs neuron-glia interactions *in vitro*, and BrdU or GFP-labeled cortical neurons in *Itga3* null mice displayed retarded radial and tangential migration or were misplaced (39, 47). α3β1 integrins also regulate interneuron migration by interacting with netrin1 (13). Our results show that *Vps18* deficiency-mediated up-regulation of β1 integrin on the cell surface impairs neuronal migration, but does not affect layer formation in cerebral cortex. We have also demonstrated that knocking down of β1 integrin mitigates the migration defects. These results also support the notion that β1 integrin has a modulatory role for neuron migration.

Because the knockdown of β1 integrin only partially rescue neuronal migration defect in *Vps18* CKO mouse brain, we suspected that there were other unknown mechanisms underlying impaired migration of *Vps18*-deficient neural cells. Radial migration of neurons is guided by radial glial fibers in the brain. Disruption of arrangement of radial glial processes led to obstruction of neuronal migration (48, 49). Therefore, we examined whether radial glial scaffold in the brain of *Vps18* CKO mice was affected. Our analysis showed that the *Vps18* deficiency resulted in severe disruption of radial glial fibers in cerebellar primordiums but no obvious defects in cerebral cortices (supplemental Fig. S1). The severity of disorganized radial glia processes in the *Vps18*-deficient cerebral cortex and cerebellar primordium is consistent with the harshness of impaired neuronal migration in these two tissues, that is, layer formation is not affected in cerebral cortices but is disturbed in the cerebellums of the *Vps18*-deficient brain. Therefore, disrupted radial glial fibers could be another factor leading to impaired neuronal migration at least in the cerebellums of *Vps18* CKO mice. However, further work is needed to elucidate the mechanism(s) by which *Vps18* specifically regulates development or maintenance of radial glia fibers in cerebellar primordiums.

REFERENCES

1. Cheung, Z. H., and Ip, N. Y. (2011) Autophagy deregulation in neurodegenerative diseases: recent advances and future perspectives. *J. Neurochem.* **118,** 317–325

2. Zhang, M. (2008) Endocytic mechanisms and drug discovery in neurodegenerative diseases. *Front. Biosci.* **13,** 6086–6105

3. Nixon, R. A. (2005) Endosome function and dysfunction in Alzheimer disease and other neurodegenerative diseases. *Neurobiol. Aging* **26,** 373–382

4. Hara, T., Nakamura, K., Matsui, M., Yamamoto, A., Nakahara, Y., Suzuki-Migishima, R., Yokoyama, M., Mishima, K., Saito, I., Okano, H., and Mizushima, N. (2006) Suppression of basal autophagy in neural cells causes neurodegenerative disease in mice. *Nature* **441,** 885–889

5. Komatsu, M., Waguri, S., Chiba, T., Murata, S., Iwata, J., Tanida, I., Ueno, T., Koike, M., Uchiyama, Y., Kominami, E., and Tanaka, K. (2006) Loss of autophagy in the central nervous system causes neurodegeneration in mice. *Nature* **441,** 880–884

6. Jalanko, A., and Braulke, T. (2009) Neuronal ceroid lipofuscinoses. *Biochim. Biophys. Acta* **1793,** 697–709

7. Felbor, U., Kessler, B., Mothes, W., Goebel, H. H., Ploegh, H. L., Bronson, R. T., and Olsen, B. R. (2002) Neuronal loss and brain atrophy in mice lacking cathepsins B and L. *Proc. Natl. Acad. Sci. U.S.A.* **99,** 7883–7888

8. Hatten, M. E. (1999) Central nervous system neuronal migration. *Annu. Rev. Neurosci.* **22,** 511–539

9. Trommsdorff, M., Gotthardt, M., Hiesberger, T., Shelton, J., Stockinger, W., Nimpf, J., Hammer, R. E., Richardson, J. A., and Herz, J. (1999) Reeler/Disabled-like disruption of neuronal migration in knockout mice lacking the VLDL receptor and ApoE receptor 2. *Cell* **97,** 689–701

10. Cooper, J. A. (2008) A mechanism for inside-out lamination in the neocortex. *Trends Neurosci.* **31,** 113–119

11. Schmid, R. S., Jo, R., Shelton, S., Kreidberg, J. A., and Anton, E. S. (2005) Reelin, integrin and DAB1 interactions during embryonic cerebral cortical development. *Cereb. Cortex* **15,** 1632–1636

12. Belvindrah, R., Graus-Porta, D., Goebbels, S., Nave, K. A., and Müller, U. (2007) β1 integrins in radial glia but not in migrating neurons are essential for the formation of cell layers in the cerebral cortex. *J. Neurosci.* **27,** 13854–13865

13. Stanco, A., Szekeres, C., Patel, N., Rao, S., Campbell, K., Kreidberg, J. A., Polleux, F., and Anton, E. S. (2009) Netrin-1-α3β1 integrin interactions regulate the migration of interneurons through the cortical marginal zone. *Proc. Natl. Acad. Sci. U.S.A.* **106,** 7595–7600

14. Kawauchi, T., Sekine, K., Shikanai, M., Chihama, K., Tomita, K., Kubo, K., Nakajima, K., Nabeshima, Y., and Hoshino, M. (2010) Rab GTPase-dependent endocytic pathways regulate neuronal migration and maturation through N-cadherin trafficking. *Neuron* **67,** 588–602

15. Rieder, S. E., and Emr, S. D. (1997) A novel RING finger protein complex essential for a late step in protein transport to the yeast vacuole. *Mol. Biol. Cell* **8,** 2307–2327

16. Nickerson, D. P., Brett, C. L., and Merz, A. J. (2009) Vps-C complexes: gatekeepers of endolysosomal traffic. *Curr. Opin. Cell Biol.* **21,** 543–551

17. Lindmo, K., Simonsen, A., Brech, A., Finley, K., Rusten, T. E., and Stenmark, H. (2006) A dual function for Deep orange in programmed autophagy in the *Drosophila melanogaster* fat body. *Exp. Cell Res.* **312,** 2018–2027

18. Sevrioukov, E. A., He, J. P., Moghrabi, N., Sunio, A., and Krämer, H. (1999) A role for the *deep orange* and *carnation* eye color genes in lysosomal delivery in *Drosophila. Mol. Cell* **4,** 479–486

19. Chi, C., Zhu, H., Han, M., Zhuang, Y., Wu, X., and Xu, T. (2010) Disruption of lysosome function promotes tumor growth and metastasis in *Drosophila. J. Biol. Chem.* **285,** 21817–21823

20. Maldonado, E., Hernandez, F., Lozano, C., Castro, M. E., and Navarro, R. E. (2006) The zebrafish mutant *vps18* as a model for vesicle-traffic related hypopigmentation diseases. *Pigment Cell Res.* **19,** 315–326

21. Sadler, K. C., Amsterdam, A., Soroka, C., Boyer, J., and Hopkins, N. (2005) A genetic screen in zebrafish identifies the mutants *vps18, nf2,* and *foie gras* as models of liver disease. *Development* **132,** 3561–3572

22. Liang, C., Lee, J. S., Inn, K. S., Gack, M. U., Li, Q., Roberts, E. A., Vergne, I.,

Deretic, V., Feng, P., Akazawa, C., and Jung, J. U. (2008) Beclin1-binding UVRAG targets the class C Vps complex to coordinate autophagosome maturation and endocytic trafficking. *Nat. Cell Biol.* **10,** 776–787

23. Richardson, S. C., Winistorfer, S. C., Poupon, V., Luzio, J. P., and Piper, R. C. (2004) Mammalian late vacuole protein sorting orthologues participate in early endosomal fusion and interact with the cytoskeleton. *Mol. Biol. Cell* **15,** 1197–1210

24. Dong, Y., Du, X., Ye, J., Han, M., Xu, T., Zhuang, Y., and Tao, W. (2009) A cell-intrinsic role for Mst1 in regulating thymocyte egress. *J. Immunol.* **183,** 3865–3872

25. Harlow, E., and Lane, D. (1999) *Using Antibodies: A Laboratory Manual,* Cold Spring Harbor Laboratory Press, Cold Spring Harbor, NY

26. Saito, T. (2006) *In vivo* electroporation in the embryonic mouse central nervous system. *Nat. Protoc.* **1,** 1552–1558

27. Shintani, Y., Wheelock, M. J., and Johnson, K. R. (2006) Phosphoinositide-3 kinase-Rac1-c-Jun NH$_2$-terminal kinase signaling mediates collagen I-induced cell scattering and up-regulation of N-cadherin expression in mouse mammary epithelial cells. *Mol. Biol. Cell* **17,** 2963–2975

28. International Mouse Knockout Consortium, Collins, F. S., Rossant, J., and Wurst, W. (2007) A mouse for all reasons. *Cell* **128,** 9–13

29. Barski, J. J., Dethleffsen, K., and Meyer, M. (2000) Cre recombinase expression in cerebellar Purkinje cells. *Genesis* **28,** 93–98

30. Yuasa, S., Kawamura, K., Ono, K., Yamakuni, T., and Takahashi, Y. (1991) Development and migration of Purkinje cells in the mouse cerebellar primordium. *Anat. Embryol.* **184,** 195–212

31. Zhou, X., Wang, L., Hasegawa, H., Amin, P., Han, B. X., Kaneko, S., He, Y., and Wang, F. (2010) Deletion of PIK3C3/Vps34 in sensory neurons causes rapid neurodegeneration by disrupting the endosomal but not the autophagic pathway. *Proc. Natl. Acad. Sci. U.S.A.* **107,** 9424–9429

32. Kunwar, A. J., Rickmann, M., Backofen, B., Browski, S. M., Rosenbusch, J., Schöning, S., Fleischmann, T., Krieglstein, K., and Fischer von Mollard, G. (2011) Lack of the endosomal SNAREs vti1a and vti1b led to significant impairments in neuronal development. *Proc. Natl. Acad. Sci. U.S.A.* **108,** 2575–2580

33. Kabeya, Y., Mizushima, N., Ueno, T., Yamamoto, A., Kirisako, T., Noda, T., Kominami, E., Ohsumi, Y., and Yoshimori, T. (2000) LC3, a mammalian homologue of yeast Apg8p, is localized in autophagosome membranes after processing. *EMBO J.* **19,** 5720–5728

34. Mizushima, N., and Hara, T. (2006) Intracellular quality control by autophagy: how does autophagy prevent neurodegeneration? *Autophagy* **2,** 302–304

35. Komatsu, M., Waguri, S., Koike, M., Sou, Y. S., Ueno, T., Hara, T., Mizushima, N., Iwata, J., Ezaki, J., Murata, S., Hamazaki, J., Nishito, Y., Iemura, S., Natsume, T., Yanagawa, T., Uwayama, J., Warabi, E., Yoshida, H., Ishii, T., Kobayashi, A., Yamamoto, M., Yue, Z., Uchiyama, Y., Kominami, E., and Tanaka, K. (2007) Homeostatic levels of p62 control cytoplasmic inclusion body formation in autophagy-deficient mice. *Cell* **131,** 1149–1163

36. Duit, S., Mayer, H., Blake, S. M., Schneider, W. J., and Nimpf, J. (2010) Differential functions of ApoER2 and very low density lipoprotein receptor in Reelin signaling depend on differential sorting of the receptors. *J. Biol. Chem.* **285,** 4896–4908

37. Hashimoto-Torii, K., Torii, M., Sarkisian, M. R., Bartley, C. M., Shen, J., Radtke, F., Gridley, T., Sestan, N., and Rakic, P. (2008) Interaction between Reelin and Notch signaling regulates neuronal migration in the cerebral cortex. *Neuron* **60,** 273–284

38. Graus-Porta, D., Blaess, S., Senften, M., Littlewood-Evans, A., Damsky, C., Huang, Z., Orban, P., Klein, R., Schittny, J. C., and Müller, U. (2001) β1 class integrins regulate the development of laminae and folia in the cerebral and cerebellar cortex. *Neuron* **31,** 367–379

39. Schmid, R. S., Shelton, S., Stanco, A., Yokota, Y., Kreidberg, J. A., and Anton, E. S. (2004) α3β1 integrin modulates neuronal migration and placement during early stages of cerebral cortical development. *Development* **131,** 6023–6031

40. Lobert, V. H., Brech, A., Pedersen, N. M., Wesche, J., Oppelt, A., Malerød, L., and Stenmark, H. (2010) Ubiquitination of α5β1 integrin controls fibroblast migration through lysosomal degradation of fibronectin-integrin complexes. *Dev. Cell* **19,** 148–159

41. Jung, A. R., Kim, T. W., Rhyu, I. J., Kim, H., Lee, Y. D., Vinsant, S., Oppen-

heim, R. W., and Sun, W. (2008) Misplacement of Purkinje cells during postnatal development in Bax knock-out mice: a novel role for programmed cell death in the nervous system? *J. Neurosci.* **28,** 2941–2948

42. Chintala, S., Novak, E. K., Spernyak, J. A., Mazurchuk, R., Torres, G., Patel, S., Busch, K., Meeder, B. A., Horowitz, J. M., Vaughan, M. M., and Swank, R. T. (2009) The *Vps33a* gene regulates behavior and cerebellar Purkinje cell number. *Brain Res.* **1266,** 18–28

43. Ostrowicz, C. W., Bröcker, C., Ahnert, F., Nordmann, M., Lachmann, J., Peplowska, K., Perz, A., Auffarth, K., Engelbrecht-Vandré, S., and Ungermann, C. (2010) Defined subunit arrangement and Rab interactions are required for functionality of the HOPS tethering complex. *Traffic* **11,** 1334–1346

44. Yu, W. H., Cuervo, A. M., Kumar, A., Peterhoff, C. M., Schmidt, S. D., Lee, J. H., Mohan, P. S., Mercken, M., Farmery, M. R., Tjernberg, L. O., Jiang, Y., Duff, K., Uchiyama, Y., Näslund, J., Mathews, P. M., Cataldo, A. M., and Nixon, R. A. (2005) Macroautophagy–a novel β-amyloid peptide-generating pathway activated in Alzheimer disease. *J. Cell Biol.* **171,** 87–98

45. Boland, B., Kumar, A., Lee, S., Platt, F. M., Wegiel, J., Yu, W. H., and Nixon, R. A. (2008) Autophagy induction and autophagosome clearance in neurons: relationship to autophagic pathology in Alzheimer disease. *J. Neurosci.* **28,** 6926–6937

46. Hook, V., Schechter, I., Demuth, H. U., and Hook, G. (2008) Alternative pathways for production of β-amyloid peptides of Alzheimer disease. *Biol. Chem.* **389,** 993–1006

47. Anton, E. S., Kreidberg, J. A., and Rakic, P. (1999) Distinct functions of α3 and αv integrin receptors in neuronal migration and laminar organization of the cerebral cortex. *Neuron* **22,** 277–289

48. Yuasa, S., Kitoh, J., Oda, S., and Kawamura, K. (1993) Obstructed migration of Purkinje cells in the developing cerebellum of the Reeler mutant mouse. *Anat. Embryol.* **188,** 317–329

49. Weiss, K. H., Johanssen, C., Tielsch, A., Herz, J., Deller, T., Frotscher, M., and Förster, E. (2003) Malformation of the radial glial scaffold in the dentate gyrus of Reeler mice, scrambler mice, and ApoER2/VLDLR-deficient mice. *J. Comp. Neurol.* **460,** 56–65